NASA Contractor Report 195030

Time-Dependent Deformation of Titanium Metal Matrix Composites

C. A. Bigelow
Federal Aviation Administration, Atlantic City International Airport, New Jersey

Y. A. Bahei-El-Din
University of Cairo, Cairo, Egypt

M. Mirdamadi
Analytical Services and Materials, Inc., Hampton, Virginia

National Aeronautics and
Space Administration
Langley Research Center
Hampton, Virginia 23681-0001

C. A. Bigelow, Y. A. Bahei-El-Din, and M. Mirdamadi

TIME-DEPENDENT DEFORMATION OF TITANIUM METAL MATRIX COMPOSITES

ABSTRACT: A three-dimensional finite element program called VISCOPAC was developed and used to conduct a micromechanics analysis of titanium metal matrix composites. The VISCOPAC program uses a modified Eisenberg-Yen thermo-viscoplastic constitutive model to predict matrix behavior under thermomechanical fatigue loading. The analysis incorporated temperature-dependent elastic properties in the fiber and temperature-dependent viscoplastic properties in the matrix. The material model was described and the necessary material constants were determined experimentally. Fiber-matrix interfacial behavior was analyzed using a discrete fiber-matrix model. The thermal residual stresses due to the fabrication cycle were predicted with a failed interface. The failed interface resulted in lower thermal residual stresses in the matrix and fiber. Stresses due to a uniform transverse load were calculated at two temperatures, room temperature and an elevated temperature of $650^{\circ}C$. At both temperatures, a large stress concentration was calculated when the interface had failed. The results indicate the importance of accurately accounting for fiber-matrix interface failure and the need for a micromechanics-based analytical technique to understand and predict the behavior of titanium metal matrix composites.

Keywords: thermal residual stresses, interface, finite element analysis, viscoplasticity, discrete fiber-matrix model

INTRODUCTION

Fiber-matrix interfaces can play a key role in the mechanical behavior of continuous fiber-reinforced metal matrix composites (MMC) [1]. Interfaces govern the mode and extent of load transfer between the fiber and matrix. To predict composite behavior, it is necessary to understand interfacial behavior, including fiber-matrix debonding. Because of the large differences that can occur in the coefficients of thermal expansion of the fiber and the matrix, large thermal residual stresses can develop in the composite during cooldown from the fabrication temperature. Due to the high operating temperatures of MMC, the time-dependent behavior of the matrix should also be accounted for. Thus, it is important to model the thermal residual stresses that may be present as well as the time- and temperature-dependent behavior of the titanium matrix to understand and predict the composite behavior.

The fiber-matrix interface plays a particularly significant role in MMC with a matrix having a high yield strength. To study the stress state governing fiber-matrix debonding, a

micromechanics analysis is required. A three-dimensional (3D) finite element (FE) program called VISCOPAC was used to conduct a micromechanics analysis. The VISCOPAC program uses a modified Eisenberg-Yen thermo-viscoplastic constitutive model to predict matrix behavior under thermomechanical fatigue (TMF) loading.

In the present paper, the capabilities of the VISCOPAC program are described, including the viscoplastic constitutive theory. To demonstrate the VISCOPAC program, a 3D FE unit cell micromechanics model is used to analyze the fiber-matrix interfacial behavior. The thermal residual stresses due to the fabrication cycle are predicted. The effects of the fiber-matrix interface failure and the time-dependent behavior of the matrix on the stress state in the unit cell are examined.

ANALYTICAL METHOD

Analytical predictions of the overall response of the composite material were performed with the VISCOPAC computer program developed by Bahei-El-Din for viscoplastic analysis of homogeneous and orthotropic materials subjected to thermomechanical loading. For homogeneous materials, the inelastic strain is predicted from the unified theory described in Appendix A. The viscoplastic constitutive theory implemented into the VISCOPAC program was developed by Bahei-El-Din, Shah, and Dvorak [2] for high temperature applications and is based on the viscoplastic theory of Eisenberg and Yen [3]. This constitutive theory is a unified theory, where creep and plasticity are combined, with a yield surface. The theory assumes the existence of an equilibrium stress-strain response which corresponds to the theoretical lower bound of the dynamic response. State variables include the equilibrium stress and an isotropic hardening function. Evolution laws of the state variables account for thermal recovery. A two-surface plasticity theory, where the two surfaces are the yield surface and the bounding surface, describe the state variables under nonproportional loading. In addition, this constitutive viscoplastic model assumes that the elastic response is rate-independent and that inelastic rate-dependent deformation takes place if the current stress state is greater than the equilibrium stress. The theory requires three elastic constants and 20 viscoplastic constants as a function of temperature. The viscoplastic constants will also be dependent upon the loading rate. These constants are described in more detail in Appendix A. By assuming the effects of thermal recovery and isotropic hardening were negligible for this material, the number of required constants is reduced to three elastic and six viscoplastic constants. These material constants include the elastic modulus (E), Poisson's ratio (ν) , the coefficient of thermal expansion (α), the yield stress (σ_{ys}), the yield stress of the bounding surface ($\bar{\sigma}_{ys}$), and the viscoplastic parameters, H_0, h, k, and p.

The overall strain of unidirectionally reinforced composite materials is evaluated from the inelastic strain of the homogeneous phases by means of elastic strain transformation factors which depend on the elastic properties of the fiber and matrix, the fiber volume fraction, and the micromechanical interaction of the phases. In the VISCOPAC program, the user has a choice of one of three averaging models: the self-consistent model [4], the Mori-Tanaka model [5], or the vanishing-fiber-diameter material (VFD) model [6, 7, 8]. Each model is briefly described in the following paragraphs.

2

The self-consistent model [4] is centered on the solution to the problem of a single fiber embedded in an unbounded homogeneous medium which is macroscopically indistinguishable from the composite. Under any uniform loading, the fiber strain is uniform. According to the basic idea of the self-consistent model, the fiber strain is assumed to be the average of the fibers in the composite.

Having noted the important role of image stress in work hardening of dispersion hardened materials, Mori and Tanaka [5] developed a method of calculating the average internal stress in the matrix of a material containing inclusions. They showed that the average stress in the matrix is uniform throughout the material and independent of the position within the domain. The actual stress in the matrix is the average stress plus the locally fluctuating stress, the average of which vanishes in the matrix. The model also considers the average elastic energy by accounting for the effects of the interaction among the inclusions and the presence of the free boundary.

The VFD model [6, 7, 8] consists of an elastic-viscoplastic matrix unidirectionally reinforced by continuous elastic fibers. Both constituents are assumed to be homogeneous and isotropic. The fibers are assumed to have a very small diameter, so that although the fibers occupy a finite volume fraction of the composite, they do not interfere with matrix deformation in the two transverse directions, but only in the axial (fiber) direction.

MATERIALS AND TEST SPECIMENS

The material modeled in this study was SCS-6/Timetal-21S which is fabricated by hot isostatic pressing (HIPing) Ti-15Mo-3Nb-3Al-0.2Si foils between tapes of unidirectional SCS-6 silicon-carbide fibers. A fiber volume fraction of 38.5% with a fiber diameter of 0.14 mm was used. The matrix material constants needed for constitutive model used in VISCOPAC were determined experimentally by testing neat Timetal-21S material that had been subjected to the same processing cycle as the composite material. Prior to testing, all test specimens were heat treated (aged) at 621°C for eight hours in vacuum to stabilize the matrix material.

EXPERIMENTAL TECHNIQUES

All experiments were conducted using a 100-kN closed-loop servohydraulic test frame equipped with water-cooled hydraulic grips. The test specimens were heated using a 5 kW induction generator with three independent coils. The induction generator was controlled by a temperature profiler capable of running predetermined temperature profiles. K-type thermocouples were used to monitor and control the temperature along a 50-mm gauge length section in the center of the specimen. In addition, an infrared thermovision camera was used to insure that the temperature distribution was uniform along the gage section of the specimen.

MATRIX MATERIAL CONSTANTS

The matrix material constants used in the VISCOPAC program are given in Table 1. These material constants include the elastic modulus (E), Poisson's ratio (ν) , the coefficient of thermal expansion (α), the yield stress (σ_{ys}), the yield stress of the bounding surface ($\bar{\sigma}_{ys}$),

3

and the viscoplastic parameters, H_o, h, k, and p. The coefficient of thermal expansion was determined from a load-controlled experiment. A test specimen, under zero load, was subjected to temperature increments ranging from -130^oC to 816^oC. At each temperature increment, the temperature was held constant (about 1 minute) to allow for stabilization. The temperatures and the corresponding thermal strains were fit to a third degree polynomial using the method of least squares. The resulting polynomial function was differentiated with respect to temperature to determine the coefficient of thermal expansion as a function of temperature. The elastic modulus and the yield stress were determined from the linear portion and the onset of nonlinearity of the stress-strain curve, respectively, at each temperature.

Strain-controlled tests were used to define the equilibrium stress-strain curves, following the procedures defined by Mirdamadi, et al. [9]. As schematically illustrated in Figure 1, to allow stress relaxation, five-minute hold periods were imposed at predetermined strain levels. At each temperature, a minimum of five strain levels were selected to construct the equilibrium stress-strain curve. The strain rate during the loading was 1×10^{-4} mm/mm/sec. The equilibrium curve was then approximated by fitting to a power law equation as described by Mirdamadi and Johnson [10]. Once the equilibrium curve is known, the constants k and p are determined by conducting a uniaxial tensile test under load control. As shown schematically in Figure 2, the overstress R is defined as the difference between the equilibrium curve and the loading curve. The inelastic strain rate $\dot{\varepsilon}_{in}$ can be written as a function of the overstress R and the constants k and p as $\dot{\varepsilon}_{in} = k\,R^p$. By plotting the inelastic strain rate $\dot{\varepsilon}_{in}$ and R on a log-log plot, the constant k is found as the y-axis intercept and the constant p is found as the slope of the plot.

The remaining viscoplastic constants, H_o, h, σ_{ys}, and $\overline{\sigma}_{ys}$, are determined from the equilibrium curve as shown in Figure 3. H_o is the slope of the bounding curve, defined by the asymptotic value of the equilibrium curve. The yield stress of the bounding curve $\overline{\sigma}_{ys}$ is defined as the y-intercept of the line defining the slope H_o. The constant h is determined from the equation of the instantaneous slope of the equilibrium curve, $H = H_o + h[\delta/(\delta_{in} - \delta)]$. Figure 4 shows the predicted stress-strain curves at three temperature, compared to the test data. The agreement between the viscoplastic theory and experiment is very good.

ANALYTICAL MODELING

The VISCOPAC program was used to analyze a discrete fiber-matrix (DFM) model assuming an infinitely repeating, rectangular array of fibers, rather than use one of the averaging models contained in the program. The VISCOPAC program uses three dimensional, eight-noded hexahedral elements and calculates the stresses at the element centroids. The ply thickness (0.104 mm), the fiber volume fraction (38.5%), and the fiber radius (0.070 mm) were used to calculate the dimensions of the model, as shown in Figure 5. The ply thickness, the fiber volume fraction, and the fiber diameter are typical for silicon-carbide/titanium matrix composites. Figure 5 also shows the finite element mesh refinement that was used. The model shown in Figure 5 was used with the appropriate boundary conditions to represent a

4

single fiber in an infinite array of fibers. For the single fiber in an infinite array, compatibility with adjacent unit cells was enforced on each face of the model by constraining all normal displacements to be equal. On the x = 0 face, the x-displacements were set to zero, on the y = 0 face, the y-displacements were set to zero, and on the z = 0 face, the z-displacements were set to zero. On the x = 0.096 mm face, the x-displacements were constrained to be equal to each other such that the plane remained plane. That is all nodes in the plane were free to move, but all nodes in that plane moved the same amount in the x-direction. Likewise for the y = 0.104-mm plane and the z = 0.02-mm plane. A convergence study was done on the mesh shown in Figure 5. For the thermal loading used here, the mesh shown in Figure 5 predicted stresses that differed by less than 5% from those predicted by a mesh with twice the refinement.

Two loading conditions were analyzed. The thermal residual stresses due to the processing cycle and the mechanical stresses due to a uniform transverse loading were calculated. Stresses were calculated assuming an intact interface and a failed interface. A perfect bond between the fiber and matrix was assumed for the intact cases. The failed interface was modeled by modifying the element properties of the layer of matrix material next to the fiber. The interface was assumed to be failed from the start of the loading, i.e., progressive damage was not modeled. A very thin layer of elements was introduced next to the fiber; the thickness of the interface was modeled as 0.0001 mm, compared to the fiber radius of 0.07 mm. To model the failed interface, the modulus of this interface layer was set to 50 MPa, compared to the room temperature modulus of the matrix of 116 GPa. To calculate the thermal residual stresses, the temperature was assumed to be uniform throughout the laminate and only the thermal cycle occurring during the fabrication process is analyzed in the present work. Thermal residual stresses were calculated assuming a temperature change of $-629^{\circ}C$; that is a temperature change from $650^{\circ}C$ to room temperature $21.1^{\circ}C$. This temperature change is approximately one half of the melting point of the Ti-15-3 matrix. It was assumed that any residual stresses that developed during fabrication of the composite would be relieved due to relaxation at temperatures greater than one half the melting point of the matrix [11]. The fiber was assumed to remain elastic with temperature dependent properties. The elastic properties of the fiber are given in Table 2.

RESULTS AND DISCUSSION

Stress contours, based on element centroid values, are plotted for both loading conditions with an intact and a failed interface.

Thermal Residual Stresses

A time period of one hour was used to simulate the fabrication process, although, since no viscoplastic behavior was predicted, the time used to simulate the cooldown cycle was immaterial. Figures 6 and 7 show the σ_{xx} stresses produced by the simulated cooldown cycle with an intact and failed interface, respectively. The dashed line shown in the figures represents the fiber-matrix boundary. For comparison purposes, the same scale for the stresses contours in used in both figures. This results in some detail being lost in Figure 6, where the stresses are greater due to the constraint provided by the intact interface. For the intact interface, Figure 6, the σ_{xx} stresses range from approximately -400 to 475 MPa. The

5

maximum tensile and compressive stresses are not shown in Figure 6 due to the stress contour levels chosen. The maximum tensile stress occurred in the upper left corner of the model and the maximum compressive stresses occurred in the lower right hand corner of the model. For the failed interface, Figure 7, the σ_{xx} stresses range from approximately -200 to 295 MPa. The intact interface results in a greater constraint between the fiber and matrix, producing larger residual stresses. Although not shown, the calculated the σ_{yy} stresses were nearly identical to the σ_{xx} stresses. If the DFM model had been symmetric, the σ_{xx} and σ_{yy} would have been identical. The transverse stresses, σ_{xx} and σ_{yy}, govern the radial and circumferential cracking in the matrix, fiber and interface region. The lower stresses in the case of the failed interface indicate a lesser propensity for matrix cracking once the interface has failed.

Figures 8 and 9 show the σ_{zz} stresses produced by the simulated cooldown with an intact and a failed interface, respectively. In Figure 8, the σ_{zz} stresses are nearly uniform in both the fiber and matrix, with a maximum compressive stress of -835 MPa in the fiber and a maximum tensile stress of 558 MPa in the matrix. In the interface region, next to the fiber, a steep stress gradient is found due to the intact interface. In Figure 9, the σ_{zz} stresses are still nearly uniform in the fiber, but with a maximum value of -768 MPa, compared to the case of the intact interface. The region of stress gradient next to the fiber is larger in the case of the failed interface and the maximum value of tensile σ_{zz} stress in the matrix is smaller for the failed interface, 487 MPa compared to the value of 558 MPa for the intact interface. Again, the intact interface produces a greater constraint between the fiber and matrix, resulting in larger thermal residual stresses. The difference between the intact and failed cases is not as great for σ_{zz} the axial stress as for the transverse stresses. The axial stress governs axial cracking in both the fiber and the matrix. The thermal residual stresses would act as a prestress that could affect the composite properties and subsequent mechanical behavior. The axial stress calculations indicate that a smaller mechanical axial load would be necessary for the failed interface compared to the intact interface to overcome the thermal residual stresses.

Mechanical Loading

A transverse loading was applied to the model shown in Figure 5. A uniform stress in the y-direction was applied to the y = 0.104-mm face with a loading rate of 2.56 MPa/sec. Two isothermal conditions were analyzed, T = 21.1 $^{\circ}$C and 650 $^{\circ}$C. Both the intact and failed interface were modeled. The loading was applied and the stress contours were plotted at time t = 200 seconds. As shown in Figure 10 for the case of intact interfaces, at this time (t = 200 sec), for T = 21.1°C the overall behavior of the composite is still within the elastic regime, while for T = 650°C, the overall behavior is well into the inelastic regime. Inelastic behavior of the matrix was determined by comparing the von Mises equivalent stress calculated at appropriate temperature to the yield stress shown in Table 2. When the von Mises equivalent stress was greater than or equal to the yield stress, inelastic behavior of the matrix was assumed. The von Mises equivalent stress σ_{vm} is defined as follows:

$$\sigma_{vm} = \sqrt{\sigma_x^2 + \sigma_y^2 + \sigma_z^2 - \sigma_x\sigma_y - \sigma_y\sigma_z - \sigma_z\sigma_x + 3(\tau_{xy}^2 + \tau_{yz}^2 + \tau_{zx}^2)}$$

6

Figures 11 and 12 show the calculated von Mises stress contours at T = 21.1°C, t = 200 seconds, for the intact and failed interface cases, respectively. The matrix yield stress at T = 21.1°C is 910 MPa. As shown in Figure 11, even though the overall stress-strain behavior is still within the elastic region, for a small portion of the matrix (the upper left hand corner of the model), the von Mises stress is greater than the matrix yield stress, indicating inelastic behavior. For the case of the failed interface, as shown in Figure 12, the matrix is well into the inelastic regime. A large stress concentration is calculated in the lower right hand corner of the model. The maximum stress calculated for the case of the failed interface is nearly five times greater than the maximum stress in the case of the intact interface.

Figures 13 and 14 show the calculated von Mises stress contours at T = 650°C, t = 200 seconds, for the intact and failed interface cases, respectively. The matrix yield stress at T = 650°C is 43.5 MPa. At this temperature, the overall stress-strain behavior is exhibiting considerable inelastic behavior, even with an intact interface. As shown in Figure 13, all of the matrix is at a stress level greater than the yield stress. A stress concentration above the fiber is calculated for the intact interface case. For the case of the failed interface (Figure 14), a stress concentration is calculated in the lower right hand corner of the model. Here the maximum stress is about 10% greater than for the intact interface case and the region of maximum stress is considerable larger than for the intact interface case. The stress in the fiber is reduced by about 20% for the failed interface, compared to the intact interface case.

Comparing the stress states with a failed interface at the two temperatures, Figures 12 and 14, shows the two stress states have very similar trends. The magnitude of the stress is more than twice as large at room temperature than at the elevated temperature. The stress states at the two temperatures with the intact interfaces, Figures 11 and 13, however, are considerably different. As shown in Figure 11, the stress state at room temperature is more uniform than at the elevated temperature, even though the magnitudes of the stresses in both cases are nearly the same.

CONCLUDING REMARKS

A three-dimensional finite element program called VISCOPAC was developed and used to conduct a micromechanics analysis of titanium metal matrix composites. The VISCOPAC program uses a modified Eisenberg-Yen thermo-viscoplastic constitutive model to predict matrix behavior under thermomechanical fatigue loadings. The analysis incorporated temperature-dependent elastic properties in the fiber and temperature-dependent viscoplastic properties in the matrix. The material model was described and the necessary material constants were determined experimentally. The predictions of matrix behavior were accurate at a range of temperatures.

A micromechanics model was used to analyze the fiber-matrix interfacial behavior. The thermal residual stresses due to the fabrication cycle were calculated. The stresses due to a transverse mechanical loading under isothermal loading conditions were also calculated. The

7

effects of the fiber-matrix interface failure and the time-dependent behavior of the matrix on the stress state in the unit cell were examined.

The thermal residual stresses produced during the fabrication of the composite were simulated by applying a thermal load of -629°C. Significant stresses were calculated due to the simulated cooldown. The failed interface resulted in lower thermal residual stresses in the matrix and fiber. There was less constraint between the fiber and matrix in this case, thus, lowering the stresses in the constituents.

Stresses due to a uniform transverse load were calculated at two temperatures, room temperature and an elevated temperature of 650°C. The extent of inelastic behavior was studied by comparing the calculated von Mises stress state to the yield stress of the matrix. At both temperatures, a large stress concentration was calculated when the interface had failed. At room temperature, the stress with the failed interface was over five times as large as the stress with the intact interface. The difference was not as great at the elevated temperature. Significant inelastic behavior was shown at both temperatures when the interface was failed, although the magnitude of the stresses was considerably lower at the elevated temperature.

The results indicate the importance of accurately accounting for fiber-matrix interface failure and the need for a micromechanics-based analytical technique to understand and predict the behavior of titanium metal matrix composites.

REFERENCES

1. Johnson, W. S.; Lubowinski, S. J.; and Highsmith, A. L.: Mechanical Characterization of Unnotched SCS-6/Ti-15-3 Metal Matrix Composites at Room Temperature. *Thermal and Mechanical Behavior of Metal Matrix and Ceramic Matrix Composites, ASTM STP 1080*, J. M. Kennedy, H. H. Moeller, and W. S. Johnson, Eds., American Society for Testing and Materials, Philadelphia, PA, 1990, pp. 193-218.

2. Bahei-El-Din, Y. A.; Shah, R. S.; and Dvorak, G. J.: Numerical Analysis of the Rate-Dependent Behavior of High Temperature Fibrous Composites. AMD-Vol. 18, *Mechanics of Composites at Elevated and Cryogenic Temperatures*, S. N. Singhal, W. F. Jones, C. T. Herakovich, and T. Cruse, Eds., Book No. G00618, 1991, pp. 67-78.

3. Eisenberg, M. A. and Yen, C. F.: A Theory of Multiaxial Anisotropic Viscoplasticity. *ASME Journal of Applied Mechanics*, Vol. 48, 1981, pp. 276-284.

4. Hill, R.: Theory of Mechanical Properties of Fibre-Strengthened Materials--III. Self-Consistent Model. *Journal of Mechanics and Physics of Solids*, Vol. 13, 1965, pp. 189-198.

5. Mori, T.; and Tanaka, K.: Average Stress in Matrix and Average Elastic Energy of Materials with Misfitting Inclusions. *Acta Metallurgica*, Vol. 21, May 1973, pp. 571-574.

6. Bahei-El-Din, Y. A.: Plastic Analysis of Metal-Matrix Composite Laminates. Ph.D. Dissertation, Duke University, 1979.

7. Bahei-El-Din, Y. A.; and Dvorak, G. J.: A Review of Plasticity Theory of Fibrous Composite Materials. *Metal Matrix: Composites: Testing, Analysis, and Failure Modes, ASTM STP 1032*, W. S. Johnson, Ed., American Society for Testing and Materials, Philadelphia, PA, 1989, pp. 103-129.

8. Dvorak, G. J.; and Bahei-El-Din, Y. A.: Plasticity Analysis of Fibrous Composites. *Journal of Applied Mechanics,* Vol. 49,1982, pp. 327-335.

9. Mirdamadi, M.; Johnson, W. S.; Bahei-El-Din, Y. A.; and Castelli, M. G.: Analysis of Thermomechanical Fatigue of Unidirectional Metal Matrix Composite. *ASTM 1156* , W. W. Stinchcomb and N. E. Ashbaugh, Eds., American Society for Testing and Materials, Philadelphia, PA, 1993.

10. Mirdamadi, M.; and Johnson, W. S.: Prediction of Stress-Strain Response of SCS-6/Timetal-21S Subjected to the Hypersonic Flight Profile, NASA TM-109026, 1994.

11. Dieter, G. E.: Mechanical Metallurgy. 2nd Ed., McGraw-Hill, New York, 1976, pp. 451-489.

12. Shah, R. S.: Modeling and Analysis of High Temperature Inelastic Deformation in Metal Matrix Composites. Ph.D. Thesis, Rensaleer Polytechnic Institute, Troy, NY, 1991.

13. Dafalias, Y. F.; and Popov, E. P.: Plastic Internal Variable Formalism of Cyclic Plasticity. *ASME Journal of Applied Mechanics*, Vol. 43, 1976, pp. 645-651.

APPENDIX A - VISCO-PLASTIC CONSTITUTIVE MATERIAL MODEL

The thermo-viscoplastic constitutive equations developed by Bahei, et al., [2] and Shah [12] were used to describe the behavior of each homogenous phase of the composite material. At low homologous temperatures, and isothermal conditions, the constitutive theory reduces to the formulation by Eisenberg and Yen [3] in a form more suitable for nonproportional loading.

The total strain rate is decomposed into elastic, thermal, and inelastic parts. The inelastic strain rate is found as a function of the overstress measured from an equilibrium yield surface which delineates the stress states that can be reached from the current state by purely elastic deformations. In the presence of kinematic and isotropic hardening, a Mises form of the current equilibrium yield surface can be written as

$$f = \frac{3}{2}(s_{ij}^* - \beta_{ij})(s_{ij}^* - \beta_{ij}) - (Y + Q)^2 \tag{A1}$$

where s_{ij}^* is the deviatoric equilibrium stress tensor, β_{ij} denotes the center of the yield surface, $Y = Y(T)$ is the temperature dependent yield stress in tension, which is independent of the loading rate, and Q is an isotropic hardening function. Figure A1 depicts the equilibrium yield surface f in the deviatoric stress space, where K_0 is the initial yield stress in shear.

Corresponding to a given stress tensor s_{ij} which lies outside the yield surface (Eq. A1), there exists an equilibrium stress s_{ij}^* which satisfies Eq. A1 and is determined as the intersection of the equilibrium surface and the line connecting the stress point and the center of the equilibrium surface β_{ij}. Hence,

$$s_{ij}^* = \left[\frac{2[Y(T) + Q(T)]^2}{3(s_{kl} - \beta_{kl})(s_{kl} - \beta_{kl})}\right]^{1/2} (s_{ij} - \beta_{ij}) + \beta_{ij} \tag{A2}$$

The effective overstress R is a measure of the distance between the actual stress point s_{ij} and the equilibrium stress point s_{ij}^* such that R vanishes if the actual stress point lies on, or falls within, the yield surface. Thus,

$$R = \frac{3}{2}[(s_{ij} - s_{ij}^*)(s_{ij} - s_{ij}^*)]^{1/2}(Y + Q)^2 \qquad if\ f(s_{ij} - \beta_{ij}) > 0 \tag{A3}$$

$$R = 0 \qquad\qquad\qquad\qquad if\ f(s_{ij} - \beta_{ij}) \le 0 \tag{A4}$$

The inelastic strain rate is found from an associated flow rule in which the strain rate is normal to the equilibrium yield surface and its magnitude is assumed to be in the form of a power law of the overstress [3]

$$\dot{\varepsilon}_{ij}^{in} = \sqrt{3/2}\, k(T) R^{p(T)} n_{ij}(s_{ij}^{*}) \qquad (A5)$$

$$n_{ij} = \sqrt{3/2}\left(\frac{s_{ij}^{*} - \beta_{ij}}{Y + Q}\right) \qquad (A6)$$

where the functions $k(T)$ and $p(T)$ are material parameters and n_{ij} is the unit normal to the yield surface (Eq. A1) at the current equilibrium stress point.

The evolution equation for Q, which includes the effect of inelastic deformation and thermal recovery on the yield stress, is given by

$$\dot{Q} = q(T)[Q_a(T) - q]\dot{\varepsilon}^{in} - b_r(T)|Q - Q_r(T)|^{n_r(T)-1}[Q - Q_r(T)] \qquad (A7)$$

The functions $q_a(T)$, $q(T)$, $b_r(T)$, $q_r(T)$, and $n_r(T)$ are temperature dependent material parameters, and $\dot{\varepsilon}^{in}$ is the effective inelastic strain rate

$$\dot{\varepsilon}^{in} = [\tfrac{2}{3}\dot{\varepsilon}_{ij}^{in}\dot{\varepsilon}_{ij}^{in}]^{1/2} = k(T)R^{p(T)}; \qquad \dot{\varepsilon}_{kk}^{in} = 0 \qquad (A8)$$

Total $(Q_r(T) = 0)$ or partial $(Q_r(T) \neq 0)$ thermal recovery is represented by the second term in Eq. (A7).

In analogy with Eq. (A7), and permitting complete thermal recovery of kinematic hardening, the evolution equation for the center of the yield surface β_{ij} can be written as

$$\dot{\alpha}_{ij} = \dot{\mu}\, v_{ij} - c_r(T)\overline{\alpha}^{-(m_r(T)-1)}\alpha_{ij} \qquad \overline{\alpha} = (\alpha_{kl}\alpha_{kl})^{1/2} \qquad (A9)$$

where $c_r(T)$ and $m_r(T)$ are material parameters. The unit tensor v_{ij} defines the direction of translation of the yield surface in the deviatoric stress space and can be specified according to the hardening rules applied in rate-dependent plasticity theories. If the Phillips hardening rule is selected then

$$v_{ij} = \dot{s}_{ij}/(\dot{s}_{kl}\dot{s}_{kl})^{1/2} \qquad \text{if } \dot{s}_{ij} \neq 0 \qquad (A10)$$

$$v_{ij} = n_{ij} \qquad \text{if } \dot{s}_{ij} = 0 \qquad (A11)$$

The factor $\dot{\mu}$ in Eq. (A9) is found from Praeger's consistency condition, $\dot{f} = 0$, when translation of the yield surface is specified by the first term in Eq. (A9). The result is

$$\dot{\mu} = \sqrt{2/3} k(T) R^{p(T)} [H(T) - q(T)[Q_a(T) - Q]] / n_{kl} v_{kl} \qquad (A12)$$

A two-surface plasticity theory [13] can be used to describe evolution of the instantaneous tangent modulus H in terms of the distance, in the deviatoric space, between the equilibrium yield surface and a bounding surface at which the instantaneous tangent modulus assumes an experimentally measured asymptotic value H_0 as shown in Figure 3. A Mises form of the equilibrium bounding surface is written as

$$f = \frac{3}{2}(\bar{s}_{ij} - \bar{\beta}_{ij})(\bar{s}_{ij} - \bar{\beta}_{ij}) - (\bar{Y} + \bar{Q})^2 = 0 \qquad (A13)$$

where $\bar{s}_{ij}$ is the bounding stress tensor, $\bar{\beta}_{ij}$ denotes the center of the bounding surface, $\bar{Y} = \bar{Y}(T)$ is the tensile bounding stress, which is independent of the loading rate, and $\bar{Q}$ is an isotropic hardening function. Figure A1 depicts the bounding surface in the deviatoric stress space, where $\bar{K}_0$ is the initial yield stress in shear.

The instantaneous tangent modulus for the quasi-static response H is then found as

$$H(T) = H_0(T) + h(T)[\delta / (\delta_{in} - \delta)]^{m(T)} \qquad (A14)$$

$$\delta = \left[\frac{3}{2}(\bar{s}_{ij} - s_{ij}^*)(\bar{s}_{ij} - s_{ij}^*) \right]^{1/2} \qquad (A15)$$

where δ_{in} is the distance between the yield surface and the bounding surface at the onset of inelastic deformation. When the equilibrium stress point lies on the bounding surface, the plastic tangent modulus assumes the asymptotic value $H_0(T)$. Parameters h_0, h, and m need to be determined experimentally as functions of temperature.

In analogy with the equilibrium yield surface, thermal recovery of isotropic as well as kinematic hardening of the bounding surface are included in the model.. The rate equations for $\bar{Q}$ and $\bar{\beta}_{ij}$ are

$$\dot{\bar{Q}} = \bar{q}(T)[\bar{Q}_a(T) - \bar{Q}]\dot{\varepsilon}^{in} - \bar{b}_r(T)|\bar{Q} - \bar{Q}_r(T)|^{(\bar{n}(T)-1)}[\bar{Q} - \bar{Q}_r(T)] \qquad (A16)$$

$$\dot{\bar{\beta}}_{ij} - \dot{\beta}_{ij} = -\dot{\mu}u_{ij} - \bar{c}_r(T)\bar{\beta}^{(\bar{m}_r(T)-1)}(\bar{\beta}_{ij} - \beta_{ij}) \qquad (A17)$$

Functions $\bar{Q}_a(T)$, $\bar{q}(T)$, $\bar{b}_r(T)$, $\bar{Q}_r(T)$, $\bar{n}_r(T)$, $\bar{c}_r(T)$, and $\bar{m}_r(T)$ are material parameters which must be estimated based on experimental results. The unit tensor u_{ij} defined the

13

direction of translation of the bounding surface relative to the equilibrium surface in the deviatoric stress space, as shown in Figure A1.

APPENDIX B - FAILURE CRITERIA

The form of the failure criteria specified in the VISCOPAC program depends on the type of material. For isotropic materials, the following failure envelope is specified in the stress space:

$$f = (\frac{\overline{\sigma_n}}{\sigma^\mu})^2 - (\frac{\overline{\sigma_s}}{\tau^\mu})^2 - 1.0 = 0 \tag{B1}$$

where

$$\overline{\sigma_n} = \sigma_{11}^2 + \sigma_{22}^2 + \sigma_{33}^2 - \sigma_{11}\sigma_{22} - \sigma_{22}\sigma_{33} - \sigma_{33}\sigma_{11} \tag{B2}$$

$$\overline{\sigma_s} = 3(\sigma_{12}^2 + \sigma_{13}^2 + \sigma_{23}^2) \tag{B3}$$

and σ_{ij} is the average stress in an element and σ^μ and τ^μ are the strength of the material under normal and shear stress, respectively. The failure surface given by eqs. (B1-B3) is reminiscent of the Mises yield surface but with different strength magnitudes under normal and shear stresses.

For fibrous composite materials, the user can choose among two failure criteria available in the VISCOPAC program; one based on the overall stress and one based on the fiber stress. In either case, only the axial normal stress and the longitudinal shear stress components appear in the failure criteria. Specifically, the failure envelope is given by

$$f = (\frac{\sigma_{33}}{\sigma^\mu})^2 + (\frac{\sigma_{13}}{\tau^\mu})^2 + (\frac{\sigma_{23}}{\tau^\mu})^2 - 1.0 = 0 \tag{B4}$$

or

$$f = (\frac{\sigma_{33}^f}{\sigma^{\mu f}})^2 + (\frac{\sigma_{13}^f}{\tau^{\mu f}})^2 + (\frac{\sigma_{23}^f}{\tau^{\mu f}})^2 - 1.0 = 0 \tag{B5}$$

Here σ_{ij} is the overall stress and σ_{ij}^f is the fiber stress specified in a Cartesian coordinate system $\overline{x_k}$, k = 1 ,2 ,3, such that the $\overline{x_1}$-axis coincides with the fiber direction, and $\overline{x_2}\,\overline{x_3}$ coincides with the transverse plane. The symbols σ^μ and τ^μ denote the overall strength of the fibrous composite under axial normal stress and longitudinal shear stress, respectively. Similarly, $\sigma^{\mu f}$ and $\tau^{\mu f}$ denote the fiber strength under axial normal stress and longitudinal shear stress, respectively.

Table 1 - Material Properties for Neat Timetal-21S
Stress rate of 2.56 MPa/sec

Temperature (^{0}C)	21.1	115.	482.	650.
E (MPa)	116000	116000	95851	64393
v	0.34	0.34	0.34	0.34
α (mm/mm/^{0}C)	7.52e-6	7.52e-6	10.6e-6	11.8e-6
σ_{ys} (MPa)	910.	910.	472.	43.52
σ_{ys} (MPa)	969.	969.	561.	69.
H_0 (MPa)	829.	829.	1135.	300.
h (MPa)	17111.	17111.	26168	7552
k	2.1e-21	2.1e-21	5.4e-18	2.2e-12
p	8.59	8.59	6.35	3.46

Table 2 - Elastic Properties for SCS-6 Fiber

Temperature ^{0}C	E Pa	v	α mm/mm/^{0}C
21.11	3.93E11	.25	3.564E-6
93.33	3.90E11	.25	3.564E-6
204.44	3.86E11	.25	3.618E-6
315.56	3.82E11	.25	3.726E-6
426.67	3.78E11	.25	3.906E-6
537.78	3.74E11	.25	4.068E-6
648.89	3.70E11	.25	4.266E-6
760.00	3.65E11	.25	4.410E-6
871.11	3.61E11	.25	4.572E-6
1093.30	3.54E11	.25	

16

Strain Control $\dot{\varepsilon} = $ constant

Equilibrium curve

Strain

Stress
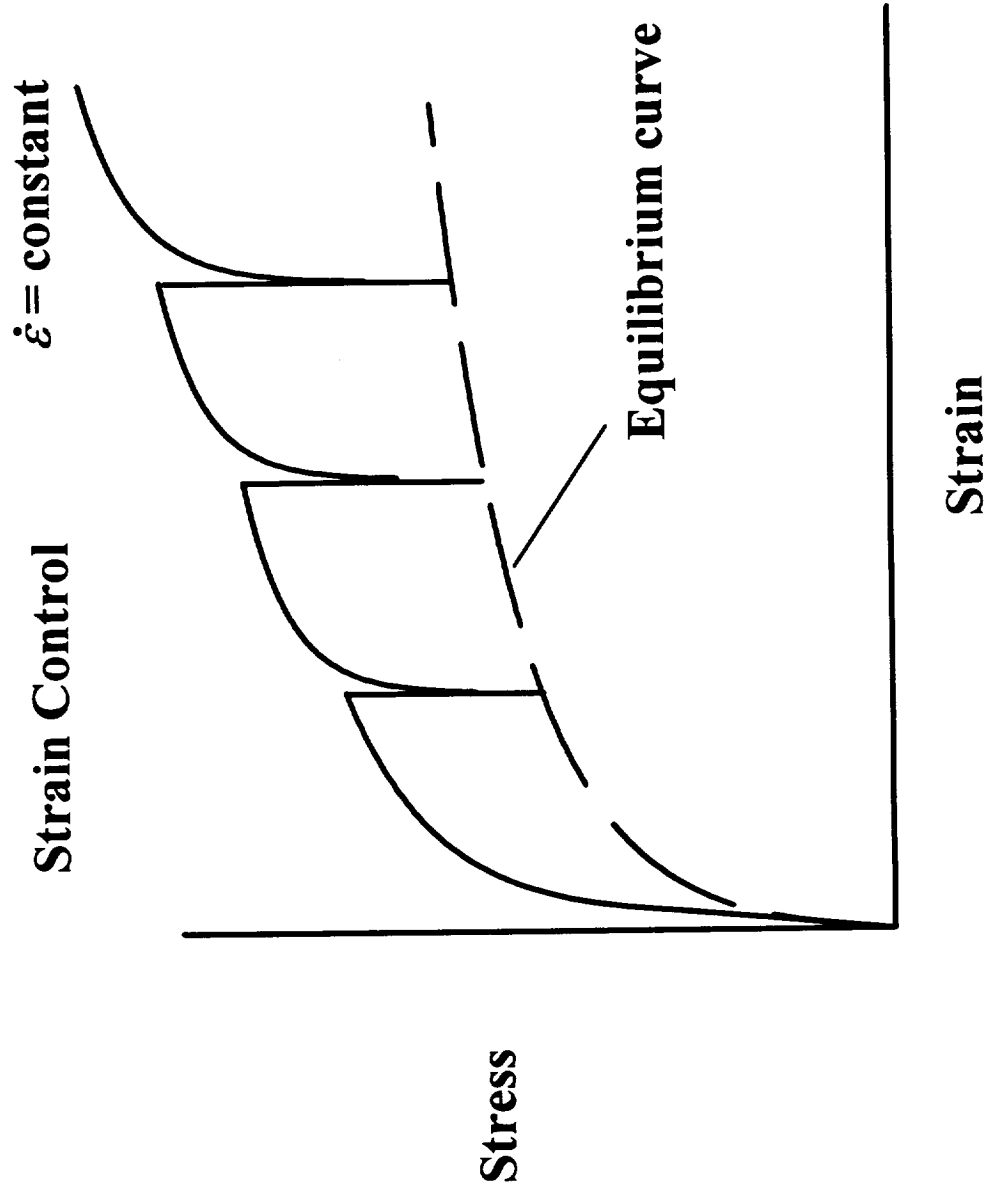
Figure 1 - Determine equilibrium curve at each temperature of interest.
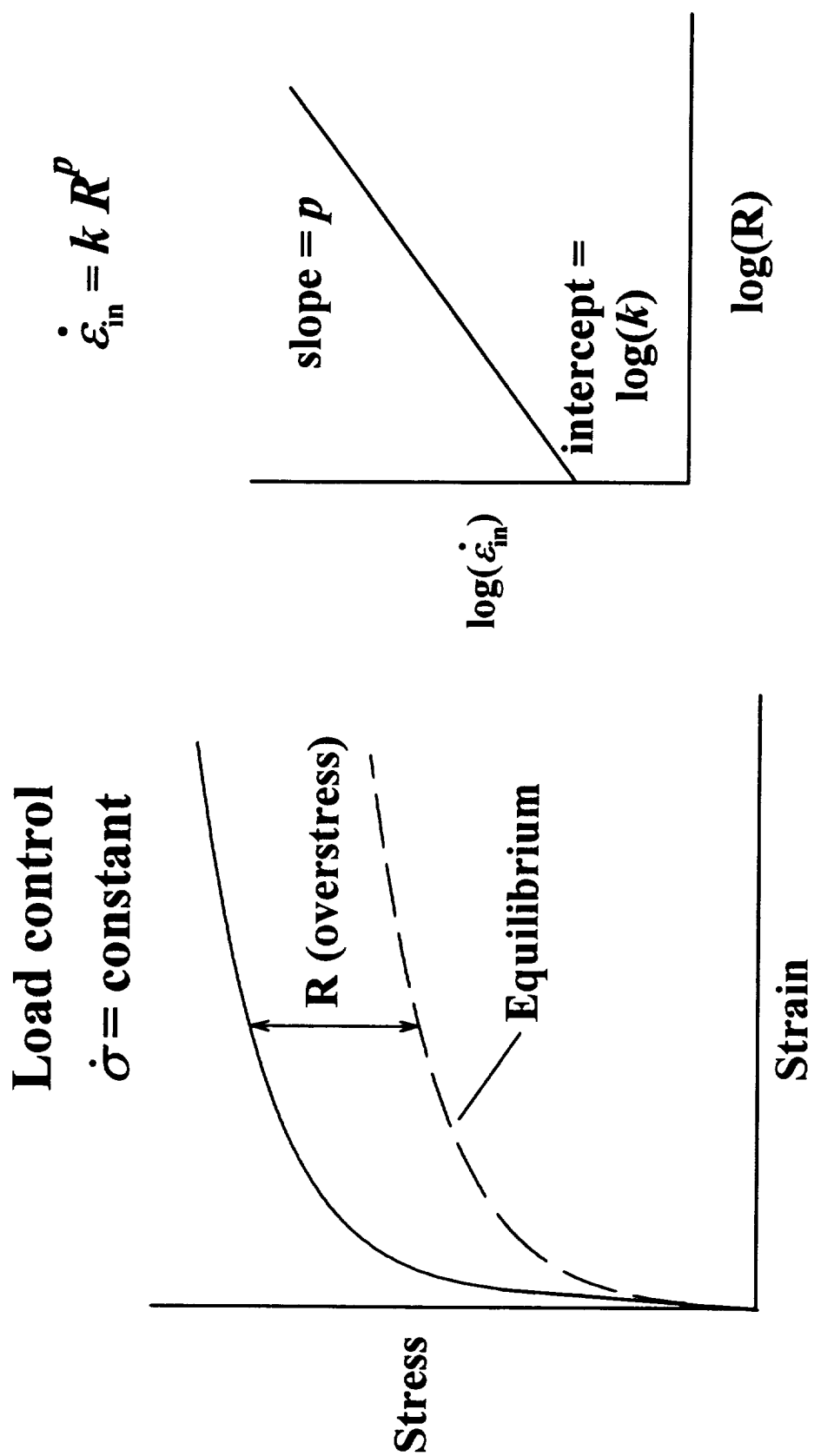
Figure 2 - Determine constants k and p at each temperature and loading rate of interest.
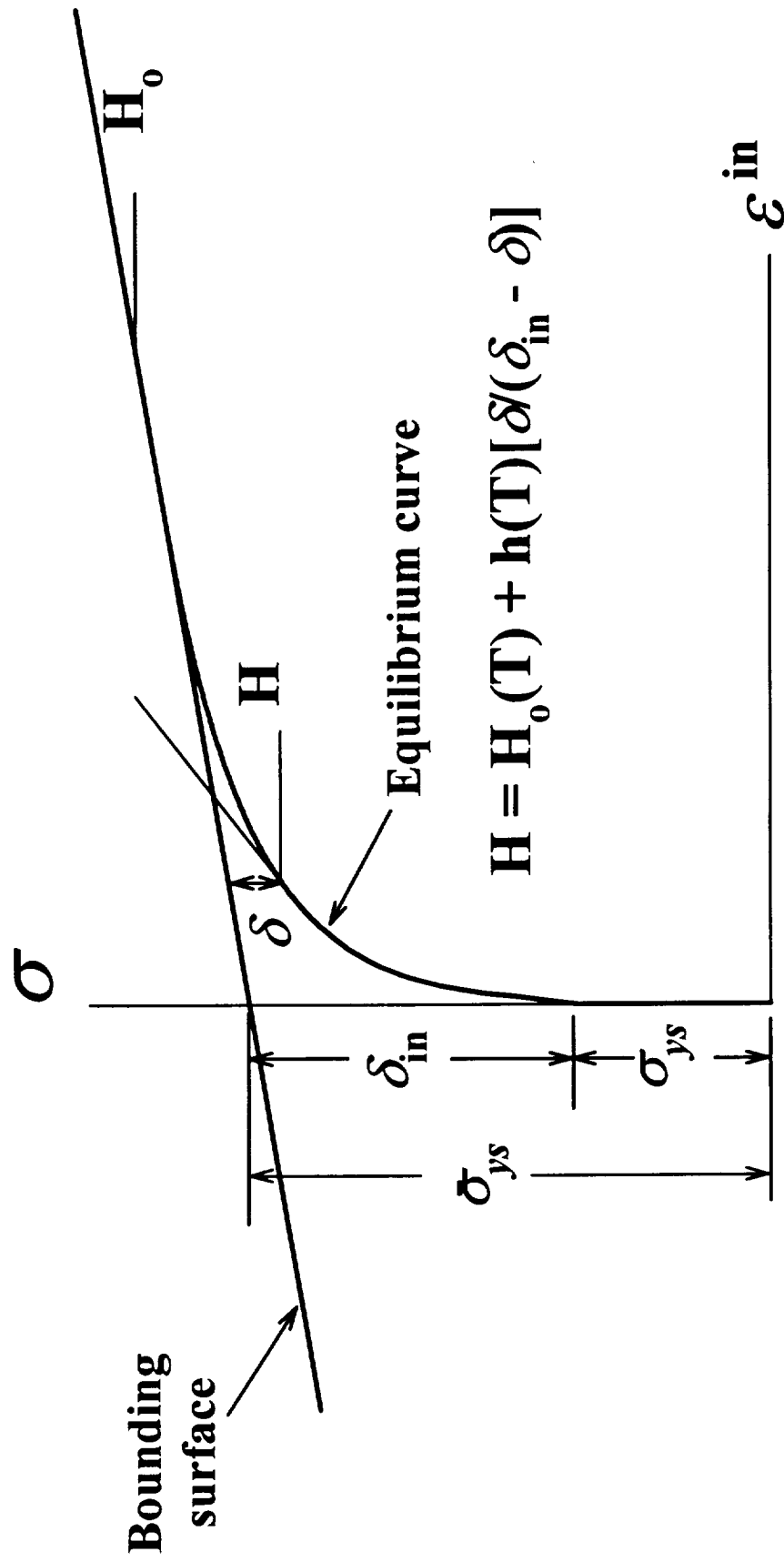
Figure 3 - Determine H_o, h, σ_{ys}, and $\bar{\sigma}_{ys}$ from equilibrium curve.

$$\mathbf{H} = \mathbf{H_o(T)} + \mathbf{h(T)}[\delta/(\delta_{in} - \delta)]$$
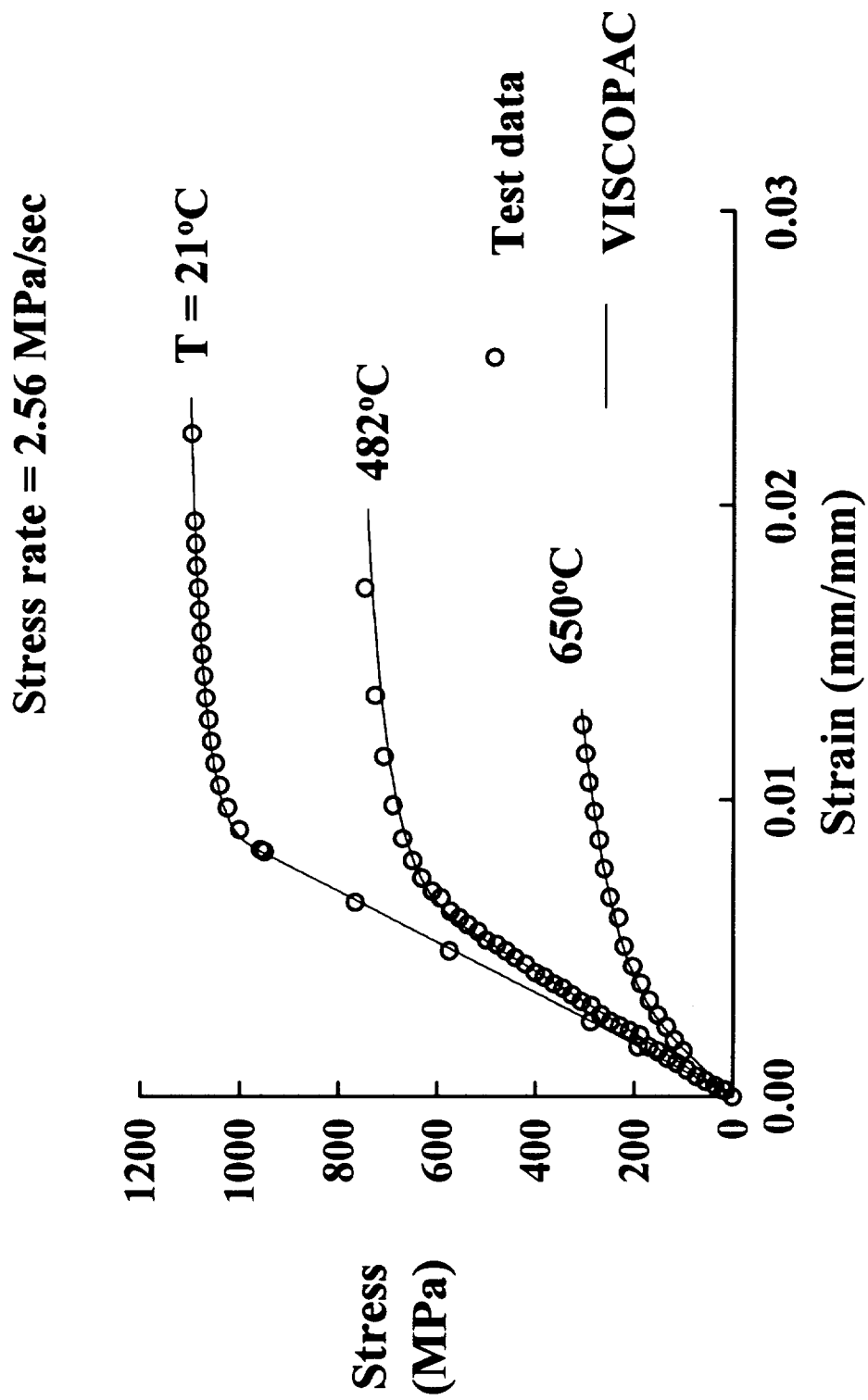
Figure 4 - Predicted matrix stress-strain curves for Timetal-21S as a function of temperature.

$v_f = 38.5\%$

y

x

z

0.02 mm

0.096 mm

0.104 mm

0.070 mm
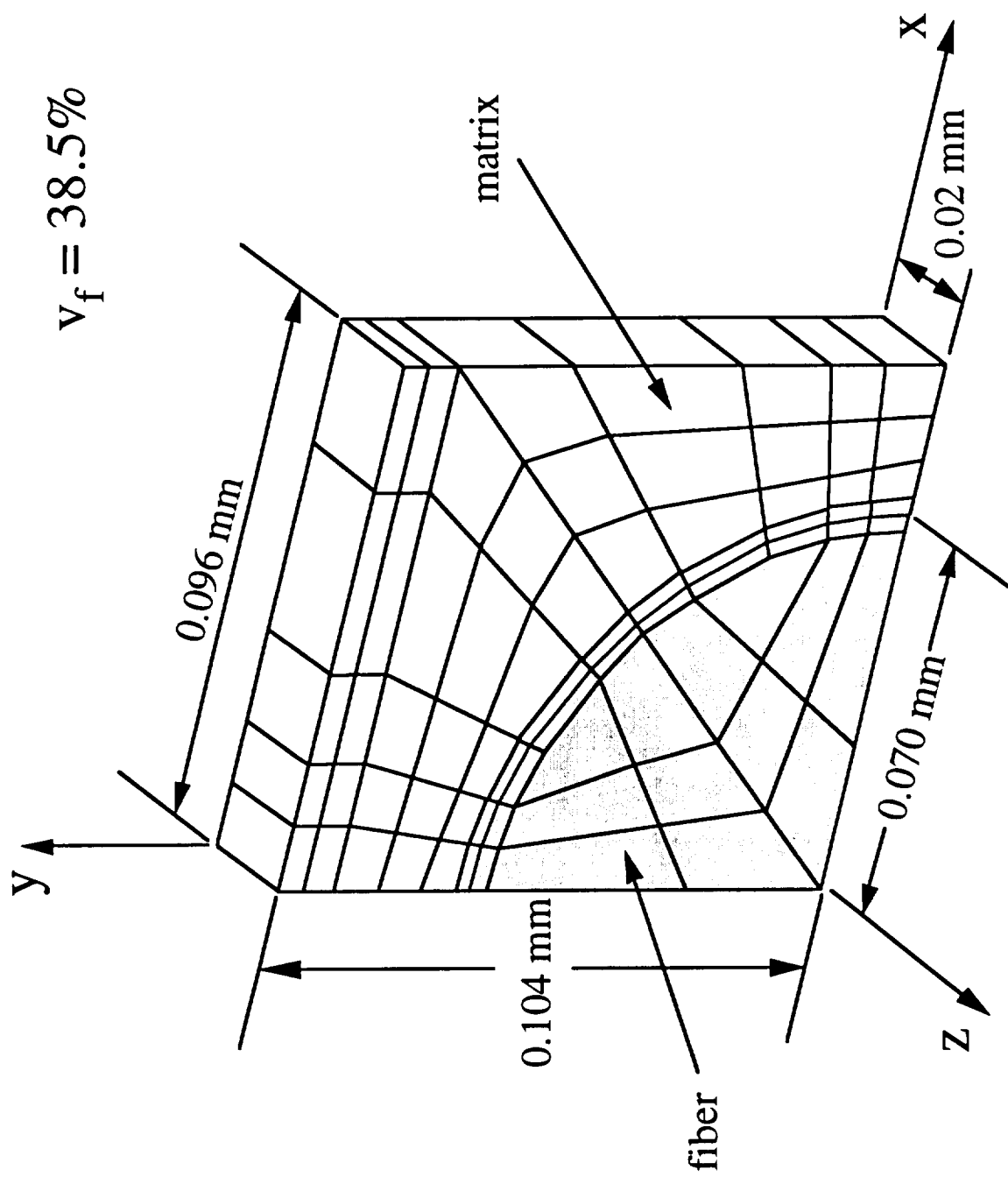
matrix

fiber

Figure 5 - Finite element mesh used to model the discrete fiber-matrix unit cell.

21

$\Delta T = -629^{\circ}C$

Level	σ_{xx} (MPa)
A	295
B	240
C	185
D	130
E	75.0
F	20.0
G	-35.0
H	-90.0
I	-145
J	-200
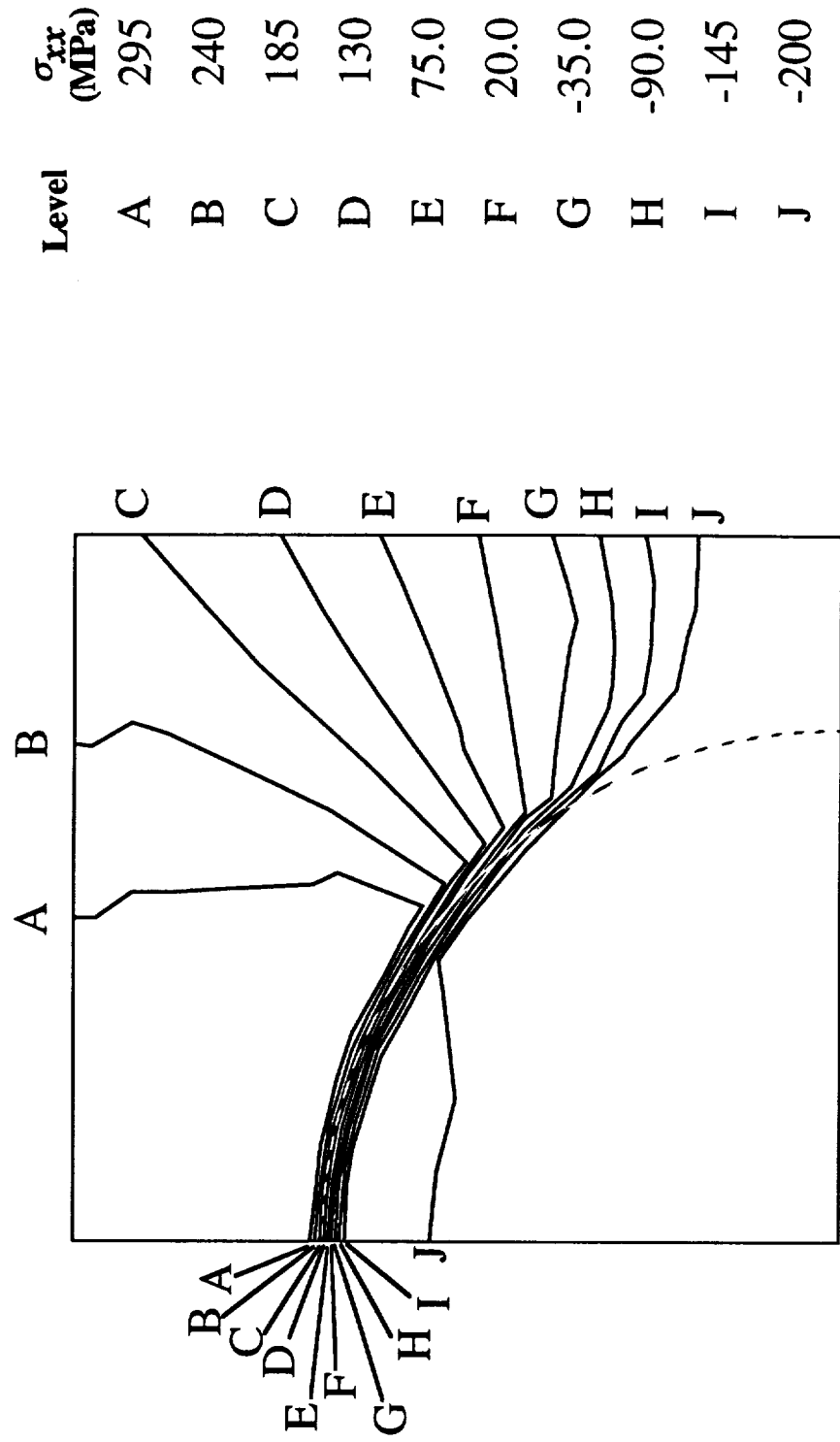
Figure 6 - Thermal residual stresses σ_{xx} with an intact interface due to simulated cooldown, $\Delta T = -629^{\circ}C$, [90] SCS-6/Timetal-21S.

$$\Delta T = -629^\circ C$$

Level	σ_{xx} (MPa)
A	295
B	240
C	185
D	130
E	75.0
F	20.0
G	-35.0
H	-90.0
I	-145
J	-200
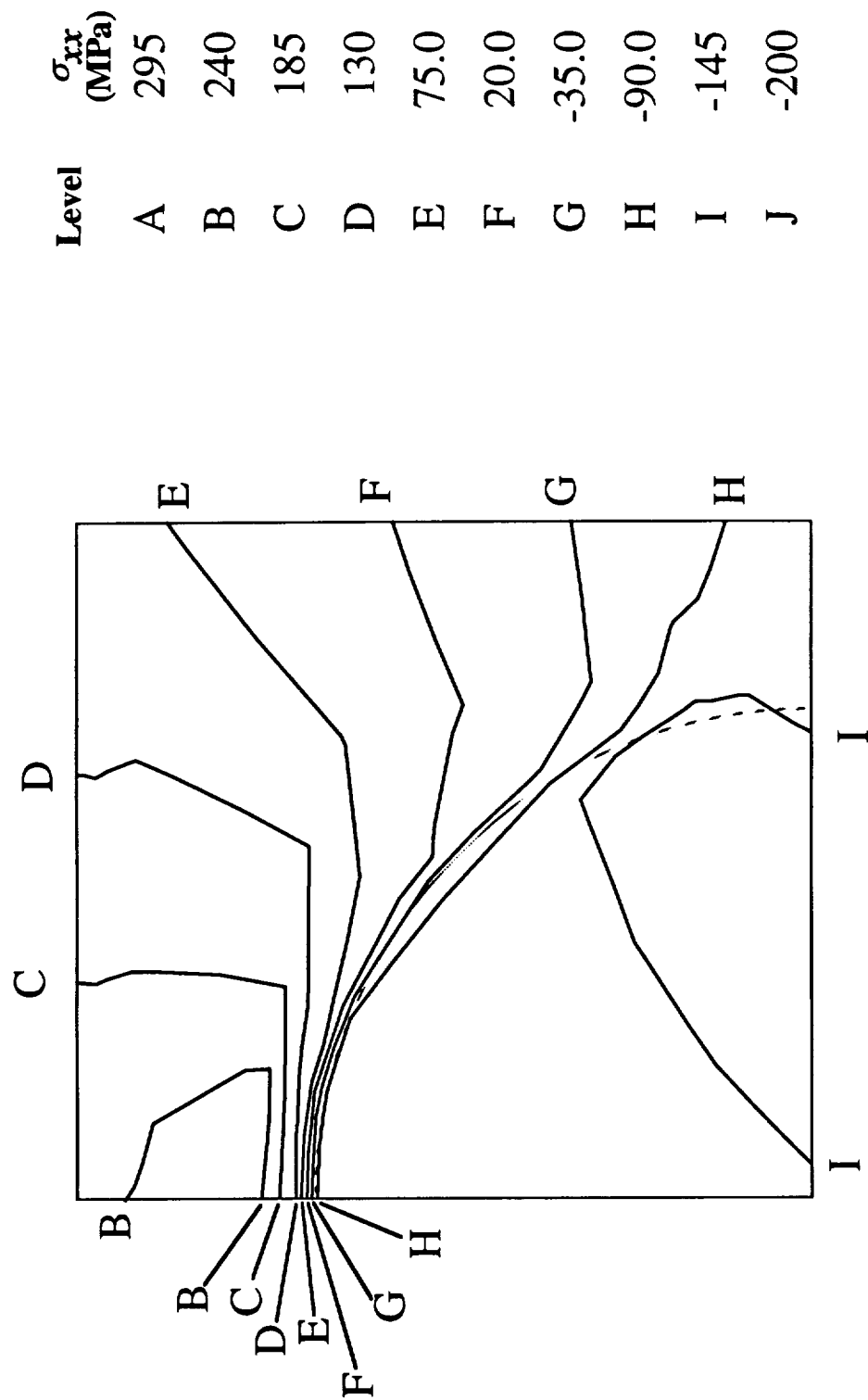
Figure 7 - Thermal residual stresses σ_{xx} with a failed interface due to simulated cooldown, $\Delta T = -629^\circ C$, [90] SCS-6/Timetal-21S.

23
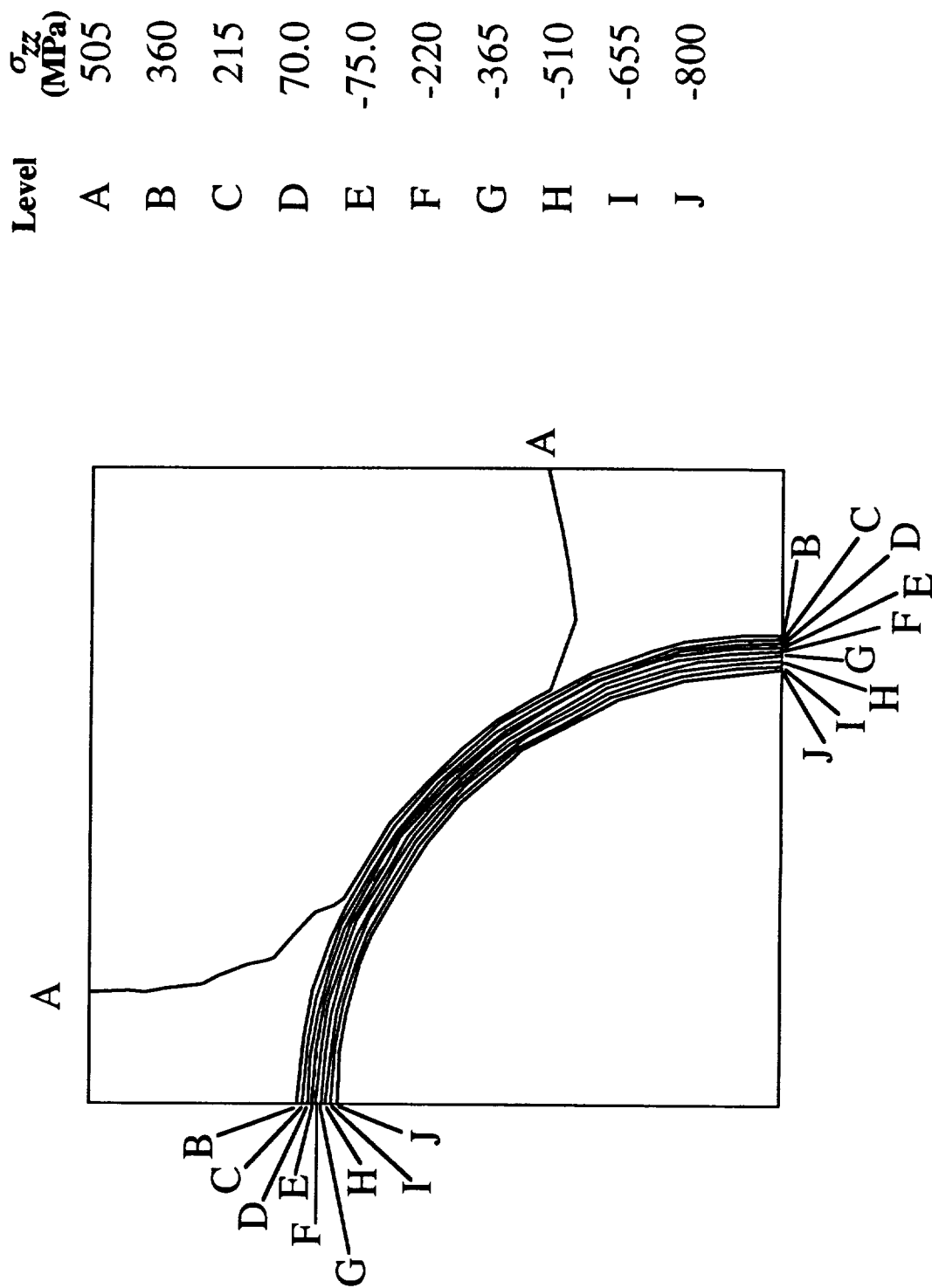
Figure 8 - Thermal residual stresses σ_{zz} with an intact interface due to simulated cooldown, $\Delta T = -629^\circ C$, [90] SCS-6/Timetal-21S.

$\Delta T = -629^{o}C$

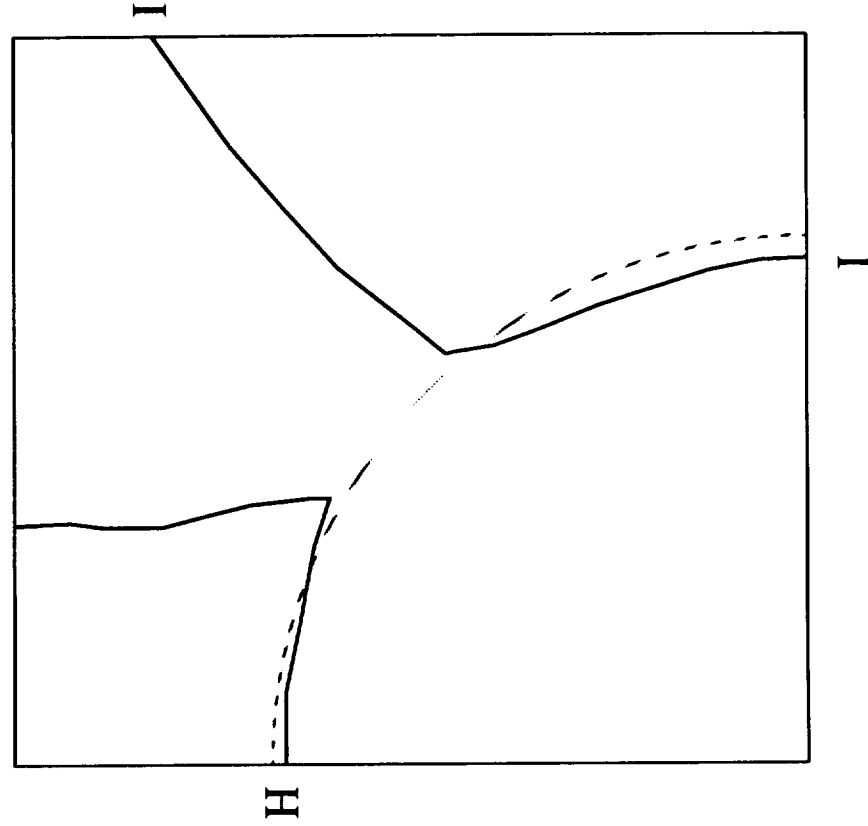| Level	σ_{zz} (MPa)
A	505
B	360
C	215
D	70.0
E	-75.0
F	-220
G	-365
H	-510
I	-655
J	-800
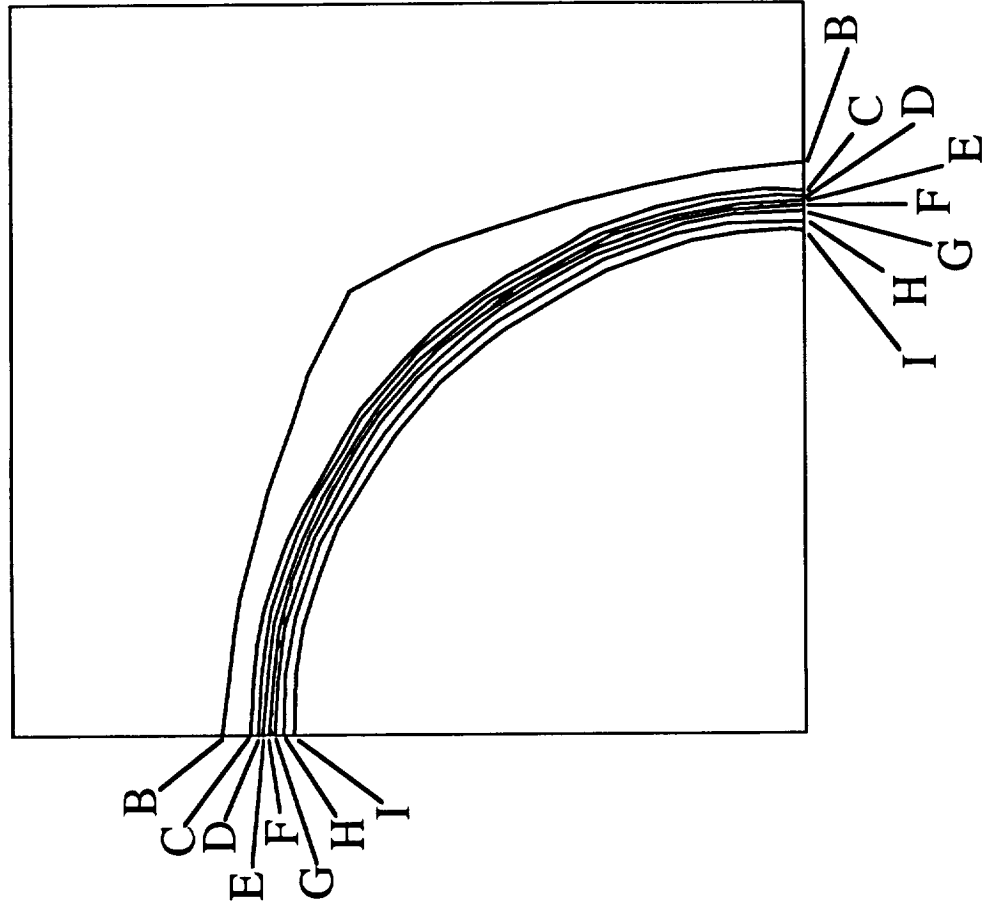
Figure 9 - Thermal residual stresses σ_{zz} with a failed interface due to simulated cooldown, $\Delta T = -629^{o}C$, [90] SCS-6/Timetal-21S.

25
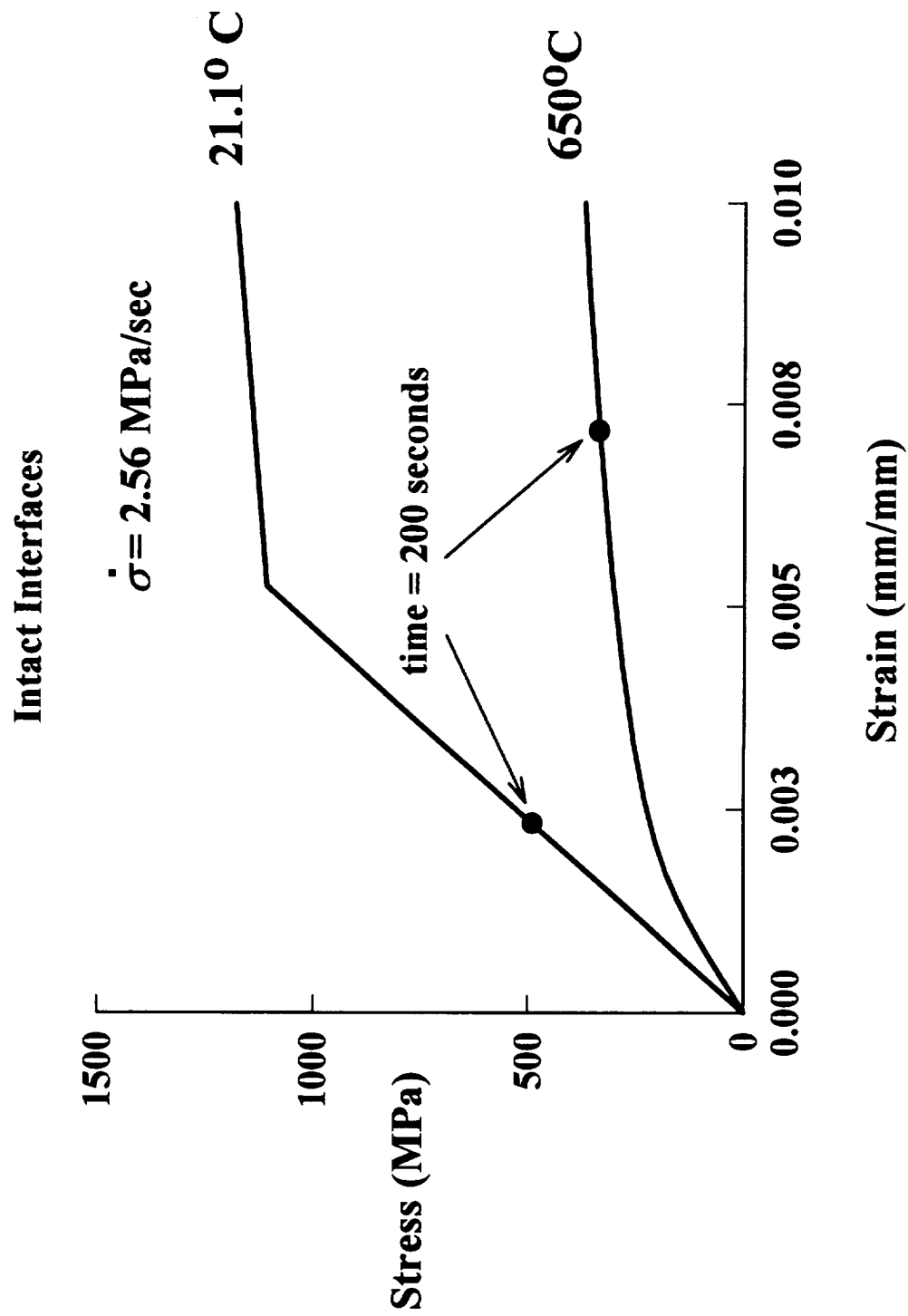
Figure 10 - Predicted stress-strain curves for [90] SCS-6/Timetal-21S with intact interfaces.
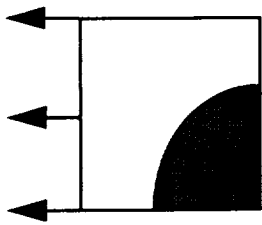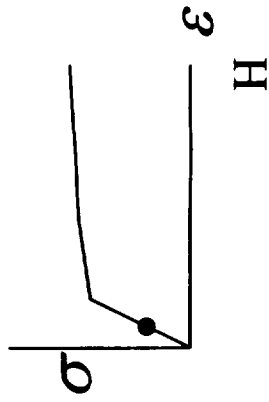
Figure 11 - Von Mises stress contours for intact interfaces, T = 21.1°C, t = 200 seconds, [90] SCS-6/Timetal-21S.
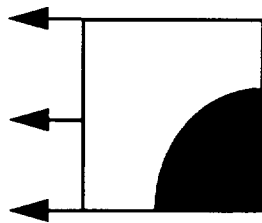
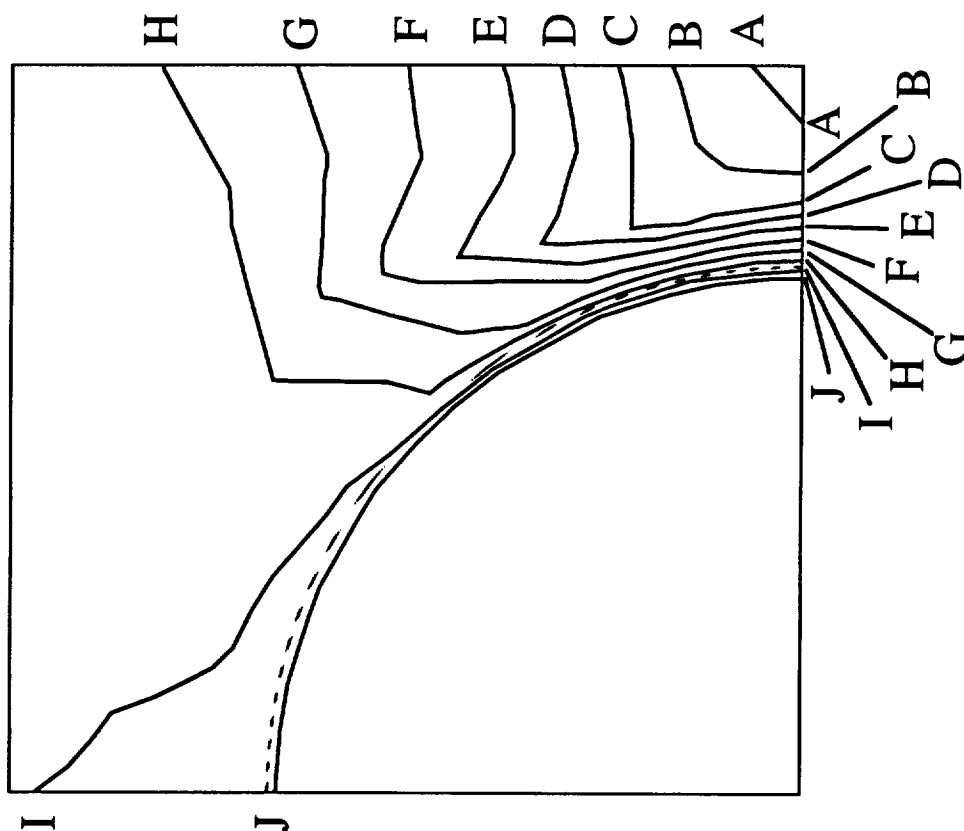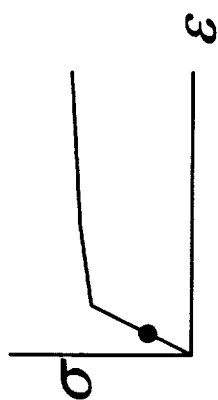Figure 12 - Von Mises stress contours for failed interfaces, T = 21.1°C, t = 200 seconds, [90] SCS-6/Timetal-21S.

$T = 650\,^{\circ}C$

$\dot{\sigma}_y = 2.56$ MPa/sec

$t = 200$ sec

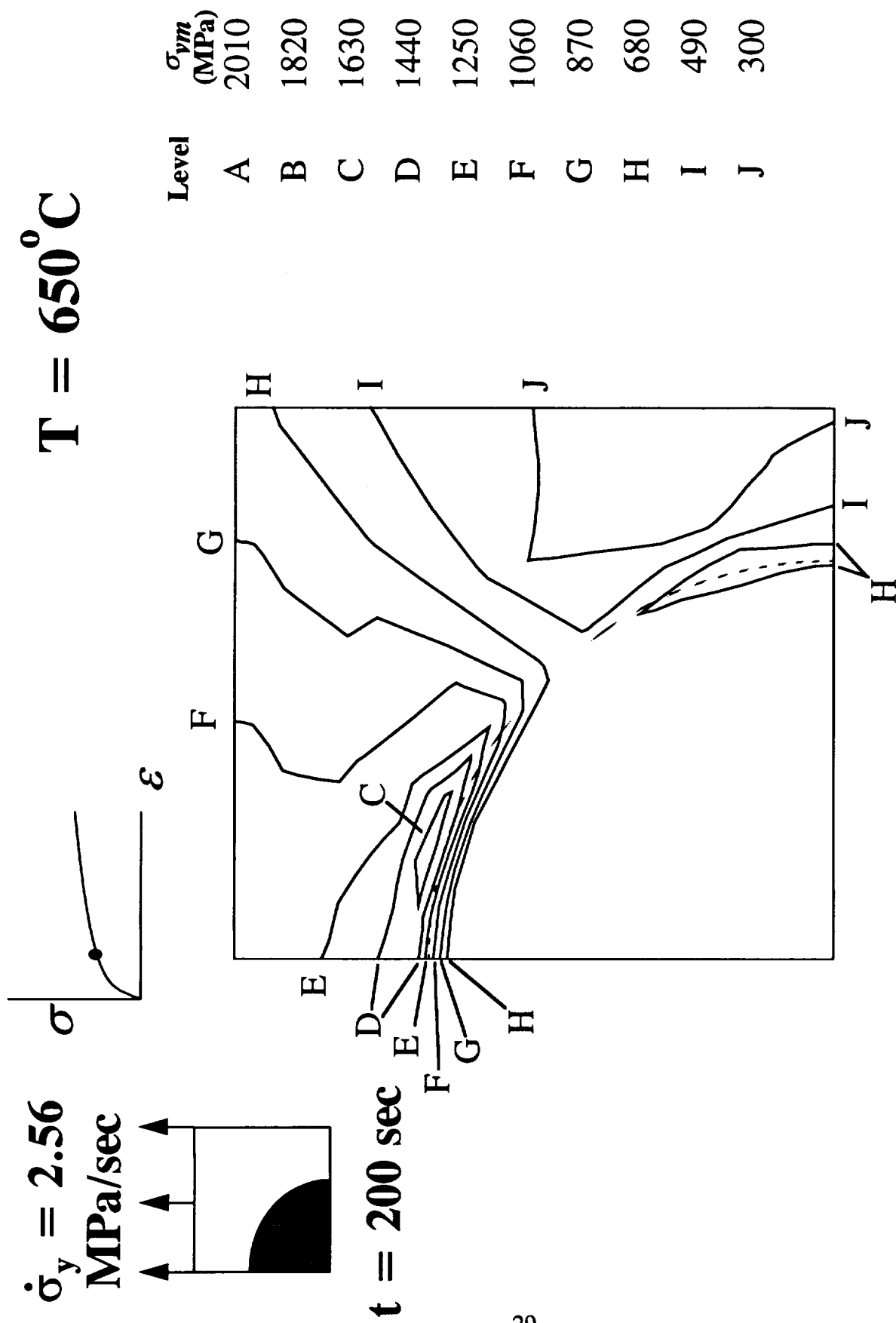| Level	σ_{vm} (MPa)
A	2010
B	1820
C	1630
D	1440
E	1250
F	1060
G	870
H	680
I	490
J	300

Figure 13 - Von Mises stress contours for intact interfaces, T = 650.°C, t = 200 seconds, [90] SCS-6/Timetal-21S.

29

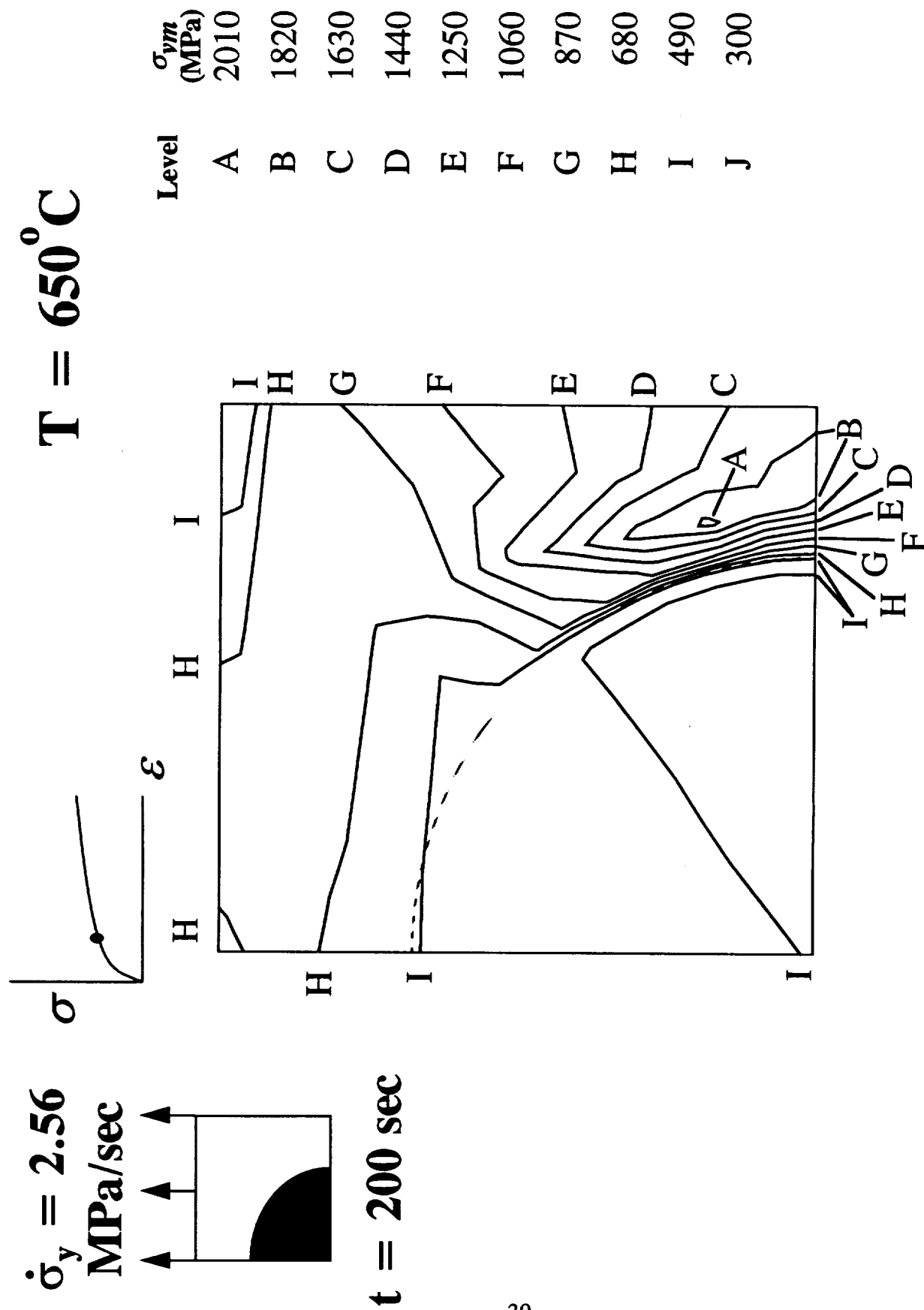Figure 14 - Von Mises stress contours for failed interfaces, T = 650.°C, t = 200 seconds, [90] SCS-6/Timetal-21S.

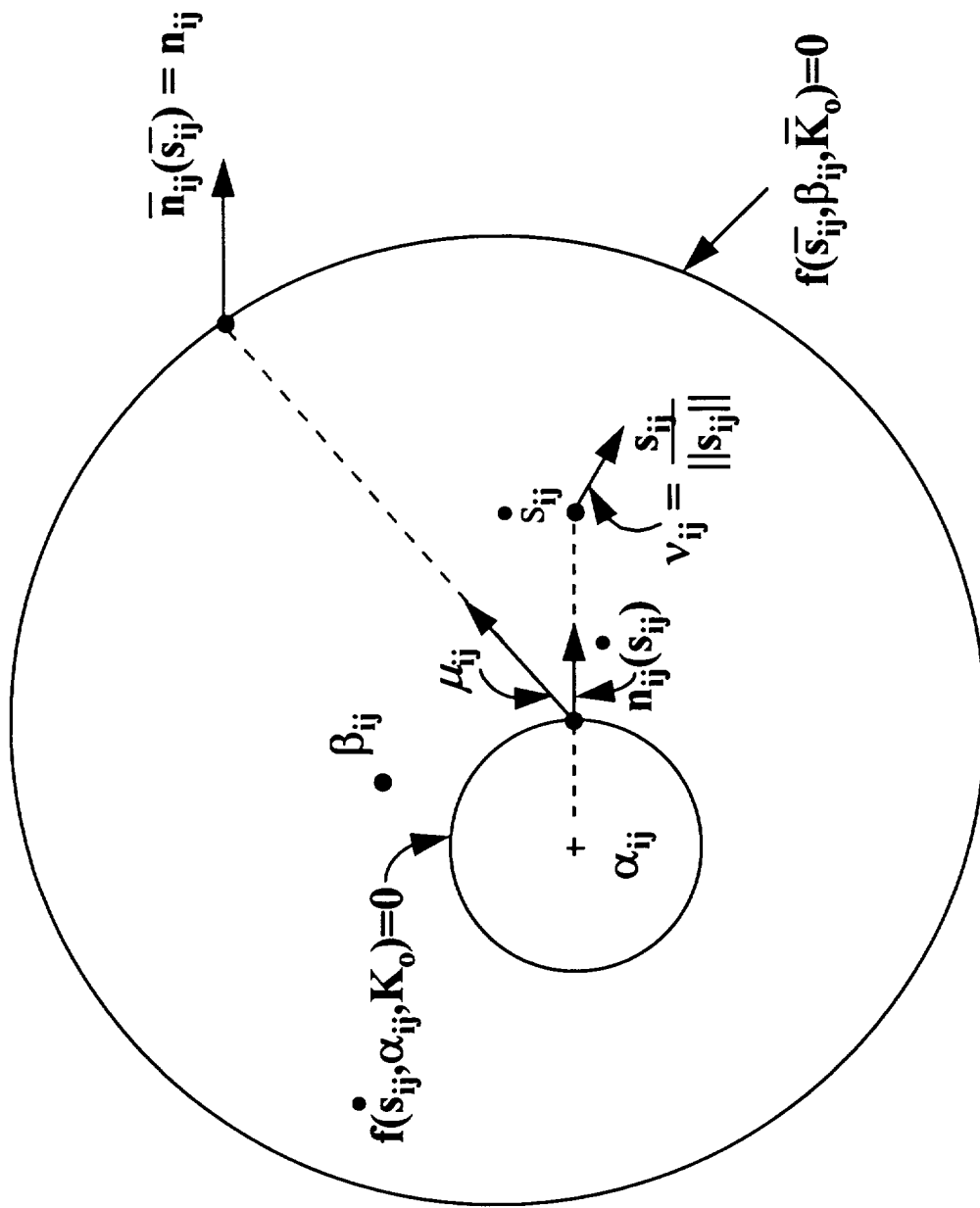| Level	σ_{vm} (MPa)
A	2010
B	1820
C	1630
D	1440
E	1250
F	1060
G	870
H	680
I	490
J	300

$\dot{\sigma}_y = 2.56$ MPa/sec

t = 200 sec

$T = 650^{\circ}C$

Figure A1 - Equilibrium and bounding surfaces in deviatoric stress space.

REPORT DOCUMENTATION PAGE

Public reporting burden for this collection of information is estimated to average 1 hour per response, including the time for reviewing instructions, searching existing data sources, gathering and maintaining the data needed, and completing and reviewing the collection of information. Send comments regarding this burden estimate or any other aspect of this collection of information, including suggestions for reducing this burden, to Washington Headquarters Services, Directorate for Information Operations and Reports, 1215 Jefferson Davis Highway, Suite 1204, Arlington, VA 22202-4302, and to the Office of Management and Budget, Paperwork Reduction Project (0704-0188), Washington, DC 20503.

1. AGENCY USE ONLY (Leave blank)	2. REPORT DATE January 1995	3. REPORT TYPE AND DATES COVERED Contractor Report

4. TITLE AND SUBTITLE

Time-Dependent Deformation of Titanium Metal Matrix Composites

5. FUNDING NUMBERS

C NAS1-19708

WU 505-63-50-04

6. AUTHOR(S)

C. A. Bigelow, Y. A. Bahei-El-Din, and M. Mirdamadi

7. PERFORMING ORGANIZATION NAME(S) AND ADDRESS(ES)

Analytical Services & Materials, Inc.
107 Research Drive
Hampton, VA 23666

8. PERFORMING ORGANIZATION REPORT NUMBER

9. SPONSORING / MONITORING AGENCY NAME(S) AND ADDRESS(ES)

National Aeronautics and Space Administration
Langley Research Center
Hampton, VA 23681-0001

10. SPONSORING / MONITORING AGENCY REPORT NUMBER

NASA CR-195030

11. SUPPLEMENTARY NOTES

Langley Technical Monitor: Ivatury S. Raju
Final Report

12a. DISTRIBUTION / AVAILABILITY STATEMENT

Unclassified - Unlimited

Subject Category 24

12b. DISTRIBUTION CODE

13. ABSTRACT (Maximum 200 words)

A three-dimensional finite element program called VISCOPAC was developed and used to conduct a micromechanics analysis of titanium metal matrix composites. The VISCOPAC program uses a modified Eisenberg-Yen thermo-viscoplastic constitutive model to predict matrix behavior under thermomechanical fatigue loading. The analysis incorporated temperature-dependent elastic properties in the fiber and temperature-dependent viscoplastic properties in the matrix. The material model was described and the necessary material constants were determined experimentally. Fiber-matrix interfacial behavior was analyzed using a discrete fiber-matrix model. The thermal residual stresses due to the fabrication cycle were predicted with a failed interface. The failed interface resulted in lower thermal residual stresses in the matrix and fiber. Stresses due to a uniform transverse load were calculated at two temperatures, room temperature and an elevated temperature of 650°C. At both temperatures, a large stress concentration was calculated when the interface had failed. The results indicate the importance of accurately accounting for fiber-matrix interface failure and the need for a micomechanics-based analytical technique to understand and predict the behavior of titanium metal matrix composites.

14. SUBJECT TERMS

Thermal residual stresses; Interface; Finite element analysis; Viscoplasticity; Discrete fiber-matrix model

15. NUMBER OF PAGES

32

16. PRICE CODE

A03

17. SECURITY CLASSIFICATION OF REPORT Unclassified	18. SECURITY CLASSIFICATION OF THIS PAGE Unclassified	19. SECURITY CLASSIFICATION OF ABSTRACT	20. LIMITATION OF ABSTRACT

NSN 7540-01-280-5500